Imaging fascicular organization of peripheral nerves with fast neural Electrical Impedance Tomography (EIT)

Enrico Ravagli[1*], Svetlana Mastitskaya[1*✉], Nicole Thompson[1*], Francesco Iacoviello[2], Paul R Shearing[2], Justin Perkins[3], Alexander V Gourine[4], Kirill Aristovich[1] and David Holder[1]

Imaging of the compound action potential (CAP) in fascicles in peripheral nerves could help avoid side effects in neuromodulation by selective stimulation of identified fascicles. Existing methods have low resolution, limited imaging depth, or are invasive. We propose fast neural electrical impedance tomography (EIT), which allows fascicular CAP imaging with a high resolution of ~200 µm, <1 ms. This uses a non-penetrating flexible cuff electrode array with 14 circumferential electrodes. This has been validated in rat sciatic nerve by comparison to micro-computed tomography (microCT) and histology with fluorescent dextran tracers (n=5). With EIT, there were reproducible localized changes in tissue impedance in response to stimulation of individual fascicles (tibial, peroneal and sural). The reconstructed EIT images corresponded to microCT scans and neural tracer histology, with significant separation between the fascicles (p<0.01), and no significant difference between techniques. The standard deviation from the mean fascicle position for EIT was 86 µm (6% of nerve diameter). This suggests fast neural EIT can reliably image the functional fascicular anatomy of the nerves and so aid selective neuromodulation.

Bioelectronic medicine, or Electroceuticals, is a rapidly developing therapeutic field in which biomedical devices are used electrically to block, record or stimulate neural activity as an alternative to drugs. A prime target for such interventions is the cervical vagus nerve which innervates various visceral organs and muscles, including the pharynx, larynx, heart, lungs and gastrointestinal tract. The human cervical vagus nerve comprises about 5-8 fascicles[1] but their anatomical relation to supplied organs is largely unknown. Until now, therapeutic electrical stimulation of the vagus nerve (VNS, vagus nerve stimulation) has been of the entire nerve. This may result in the activation of unwanted organs and so side effects, which limits therapeutic opportunities. In principle, this could be avoided by selective stimulation of specific fascicles, but this is currently not possible due to the lack of understanding of fascicular function.

Currently, there is no technique that allows for non-invasive imaging and tracing of organ-specific projections of the vagus nerve in large mammals. Neural tracing allows labelling of the cell bodies of neurons projecting to an innervated organ, but this may not label the axons[2] and requires post-mortem examination with histology and serial computerized stitching and tracking. Optical coherence tomography, photoacoustic tomography, and magnetic resonance imaging have low resolution and penetration depth[3], and multielectrode arrays are damaging to the nerve[4]. High-resolution ultrasound provides a good axial resolution of up to 400 µm but has a low soft tissue contrast which does not enable differentiation between fine nerve structures such as the fascicles and intrafascicular perineurium[5]. Magnetic resonance neurography provides good soft tissue contrast but has a spatial resolution of 0.4-0.8 mm which is insufficient for imaging of fine fascicular structures. This may be increased by imaging small fields of view and applying high magnetic fields but then there is a restricted field of view[6]. Phase contrast radiography demonstrates the fascicular nerve architecture[7] but does not enable tracking of fascicular functional connections over tens of cm.

Potential *ex vivo* methods for imaging the fascicular anatomy of nerves include histology and micro-computed tomography (microCT). Histological examination after appropriate staining may be used to study the microanatomy of tissues and trace functional connections of nerve fascicles to their end organs[8]. It requires fixation of the tissue, staining and microscopy with computerized tracking of numerous serial sections. It is accepted as a gold-standard technique but is time-consuming and may be prone to artefacts. MicroCT utilizes X-rays and provides tomographic imaging with a spatial resolution up to 4 µm in three dimensions with little distortion of the sample and minimal artefacts[9]. For application to imaging of soft tissues, including nerves, it requires the use of X-ray contrast agents such as Lugol's iodine solution, which cannot be used *in vivo*. The method has previously been applied to nerves[10,11]. However, these required phase contrast scanners and long preprocessing, which was not practical for tracking of long segments of nerve needed for delineation of functional anatomy of fascicles and their projections to the end organs. The method has been optimized in our group[12]. Using a conventional microCT scanner, it was possible to image fascicles in rat sciatic and pig vagus nerve to a length of 4 cm with a resolution of 4 µm.

Neural tracing followed by histological examination has been successfully used to study neural connections within the central and peripheral nervous system. Usually, in the PNS, tracer is applied to the peripheral organ or tissue. The majority of tracers are rapidly transported to the cell bodies of

[1]Medical Physics and Biomedical Engineering Department, University College London, London WC1E 6BT, U.K. [2]Electrochemical Innovation Laboratory, Chemical Engineering, University College London. [3]Structure and Motion Laboratory, Royal Veterinary College. [4]Centre for Cardiovascular and Metabolic Neuroscience, Neuroscience, Physiology and Pharmacology, University College London. *These authors contributed equally: E. Ravagli, S. Mastitskaya and N. Thompson. ✉e-mail: s.mastitskaya@ucl.ac.uk

projecting neurons and do not easily allow labeling of the axon shafts (e.g. horse radish peroxidase, FluoroGold, FastBlue, Diamidino Yellow)[2]. To our knowledge, there is no systematic study assessing the efficiency of neural tracers for axonal labelling at the mid-shaft of the nerve. A suitable tracer for fascicular labelling and end organ tracing should not be neurotoxic and allow practicable labelling at a defined time. Tracer toxicity appears to be poorly understood. In rat sciatic nerve, toxicity and effect on motor function was studied for FluoroGold (FG), TrueBlue (TB) and Fluoro-Rubi (FR)[13]. Both FG and TB caused functional impairment and axonal degeneration which were only reversible by week 4 (TB) or week 24 (FG) post-injection, whereas FR (which is a dextran conjugate) did not cause functional deficits and was comparable to vehicle injection[13]. Dextran conjugates are hydrophilic polysaccharides, non-toxic and relatively inert; they are transported by passive diffusion[14] and rapidly fill up the entire length of the axon when injected into the distal end of the nerve. Other tracers able to reliably label the axons without affecting the CAP are adeno-associated viral vectors (AAVs). However, AAVs require a long incubation time and are mostly efficient for anterograde tracing (from cell body to the nerve terminal)[15]. Towne et al[16] successfully traced the motor neurons in rat sciatic nerve using AAV6-mediated delivery of fluorescent reporter gene into motor neurons – the efficiency of retrograde transport reached 80-90% after intra-muscular injections of the viral vector into gastrocnemius or tibialis anterior muscle. However, to achieve successful transfection, the injections had to be made in neonates, and incubation time took four weeks.

Fast neural EIT. Electrical Impedance Tomography (EIT) is a non-invasive technique which allows imaging of variations in electrical impedance inside a volume of interest. It is achieved by mathematical reconstruction of electrical impedance data collected from an array of external electrodes[17]. Its clinical utility has been demonstrated for monitoring lung function[18], and research is in progress into its potential use in breast cancer[19], stroke[20,21], and detection of epileptic seizure onset zones[22]. It can also serve as a means to produce high resolution tomographic images of activity in excitable neural tissue in brain and nerve with a millisecond and submillimeter resolution, "fast neural EIT". Our group has developed this for imaging neuronal depolarization in the brain during normal and epileptic activity with a resolution of 1 ms and <200 µm in rat cerebral cortex[23,24]. The principle is that impedance in neuronal membranes falls as ion channels open during evoked activity. This produces a decrease in the bulk electrical impedance of ~0.1% during neuronal depolarization, which allows the applied EIT current to pass into the intracellular space, whereas at rest the EIT current predominantly travels in the extracellular space.

In fast neural EIT of peripheral nerve, the changes of electrical impedance are imaged with a cuff-like circumferential array of electrodes placed around the nerve[25]. Images are reconstructed from a set of transfer impedances. These are collected by applying a sub-threshold alternating current (AC) of ~50 µA at ~6 kHz constant current to two electrodes placed near-diametrically, generally ~100° apart; 12 voltages from all other available electrodes in the ring are recorded. Typically, impedance epochs are produced over 200 ms by averaging during 300 compound action potentials at 5 Hz elicited by supramaximal stimulation of a peripheral branch of the nerve over 60 s. A full dataset for image reconstruction is then collected by sequential switching between all possible 14 electrode pairs with the same spacing, using electronic multiplexers. The applied frequency of 6 kHz provides the optimal balance between contamination with endogenous potentials at lower frequencies and a decrease in the impedance response to depolarization at higher frequencies, both empirically and by biophysical modelling[26,27]. The resulting dataset allows imaging of neuronal depolarization with a high spatio-temporal resolution of <1 ms and 200 µm in rat sciatic nerve[25]. Optimization of related technical aspects has included electrode design and fabrication[28], current injection protocols[29], and EIT frequency range[30]. The data in this study were collected with the "UCL ScouseTom" EIT system[31]. This comprises a commercial high specification EEG recorder able to record potentials in parallel over up to 128 channels, a commercial low noise constant current generator and a custom multiplexer and controlling software.

Fast neural EIT has unique potential for identification and localization of activity within peripheral nerves. This could help to delineate functional fascicular anatomy, by indicating specific fascicles active in synchrony with individual organs or their supplying peripheral branches. The vision is that it could be left chronically *in situ* and allow imaging of fascicles of interest by gating to physiological organ activity (e.g. the ECG for heart, respiration for lung or Electrogastrogram for stomach). A pair of second nerve cuffs with identical geometry could then be used for selective stimulation and avoidance of off-target effects. It could also have practical applications in reconstructive nerve surgery as a method for functional tractography for correct fascicular repair[32] and in human robotics[33,34].

Purpose. The method of fast neural EIT applied to peripheral nerve has been published but was a technical illustration of the method in the sciatic nerve without independent validation and only of two fascicles – the posterior tibial and peroneal[25,29]. In this work, we present the first study in which the final optimised method was independently validated against histology with fluorescent dextran neural tracers and microCT. This was achieved in all three main fascicles in the rat sciatic nerve. A secondary purpose was to refine the gold standard methods of neural tracer histology and microCT to be suitable for this comparison. These are mature techniques but some development was needed to apply them successfully to fascicle tracking over several cm.

Experimental design. The compound action potential in three main fascicles of the sciatic nerve in the thigh of anesthetized Sprague-Dawley rats was imaged using fast neural EIT, using a cylindrical cuff with 14 electrodes arranged in a ring and supramaximal electrical stimulation of the tibial, peroneal and sural peripheral branches (Fig. 1). To select a robust method for neural tracing, in preliminary studies we evaluated eight different tracers, three conventional fluorescent tracers and five viral vectors. FG and DiI allowed reproducible labelling of the fascicles but

impaired evoked CAPs, which obviated reproducible EIT data. Five AAVs tested did not produce reliable results at 5-6 weeks after injection, whereas dextran tracers were reliable from the outset. We therefore opted for fluorescent dextran conjugates. These are non-toxic sugar-based tracers which travel reliably proximally in the nerve by passive diffusion, and application of these tracers did not reduce the CAPs. As only two colors were available, this was applied to the posterior tibial and peroneal fascicles. On histological examination, the third (sural) fascicle was identified as the main unstained fascicle. The experimental timeline was as follows:

- 48 h before the EIT experiment, the animal received fluorescent dextran tracer injections into the tibial and peroneal branches (Fig. 1a).
- EIT experiment: tibial, peroneal and sural branches were electrically stimulated supramaximally at 5 Hz. EIT was recorded using a cuff electrode array placed around the sciatic nerve in the thigh (Fig. 1b).
- *Post-mortem*, the nerve was removed and the entire length of several cm was imaged with microCT in order to identify the origin of each fascicle in the thigh portion of the nerve (Fig. 1c) and processed for histology (Fig. 1d).
- Resulting images from EIT, microCT, and histological slices were co-registered for statistical analysis (Fig. 1e).

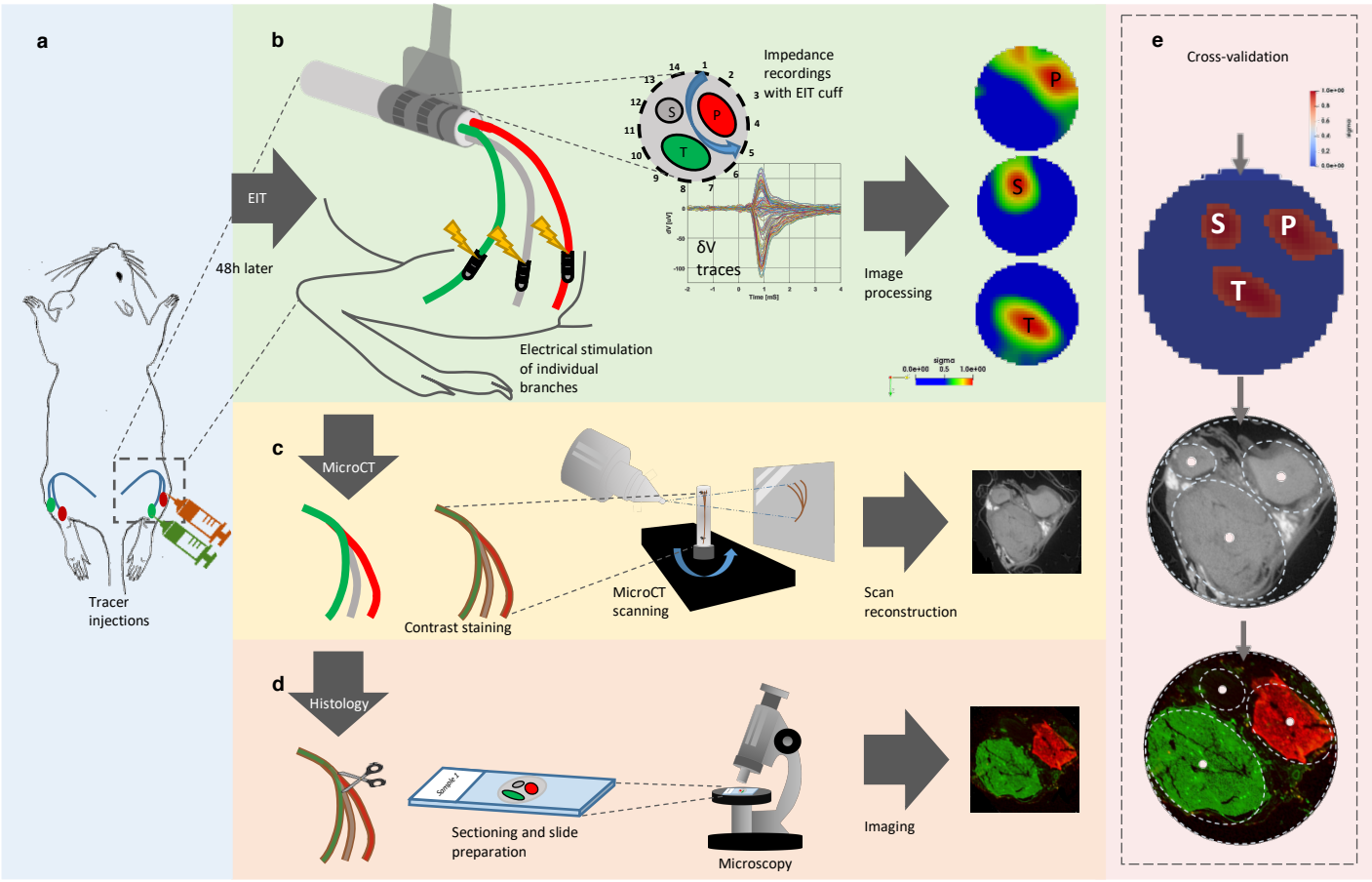

Fig. 1. Experimental design. a, Neural tracers were injected into the peroneal and tibial fascicles of the rat sciatic nerve 48h before the EIT experiment. **b**, EIT recordings and image reconstruction. *Left*: peroneal (red), tibial (green) and sural (grey) fascicles were electrically stimulated with bipolar electrodes placed 1-1.5 cm distally from the EIT cuff. *Middle*: diagram showing the 4-off electrode spacing configuration in the 14-electrode cuff forming a full ring around the rat common sciatic nerve; example of multiple δV traces from an experimental EIT recording. *Right*: Exemplar cross-sectional localization of the recorded fascicular activity from tibial (T), peroneal (P) and sural (S) fascicles at the level of the common sciatic nerve. The range of values for every image was normalized between 0 and 1 and the rainbow color scale indicates the top 50% of color for each image i.e. full width at half maximum (FWHM) intensity scaling. **c**, After the EIT experiment, the nerve was scanned with microCT. **d**, Fluorescent microscopy of histological sections. **e**, Cross-validation of EIT images of impedance changes in individual fascicles against microCT and histological sections.

Results

Compound action potentials and impedance changes in individual fascicles. CAPs of 211±142, 168±90, and 114±39 μV (peak impedance changes of 9.7±5.5 μV (0.04±0.02%), 13.7±15.8 μV (0.05±0.04%), and 13.4±11.3 μV (0.05±0.03%) with onset times of 0.7±0.2, 0.8±0.1 and 0.8±0.1 ms for tibial, peroneal and sural fascicles, respectively. All were significant with respect to baseline noise (paired t-test with respect to inter-stimulus noise, $p<0.05$) (Fig. 2). The duration above 30% of peak impedance change was 0.7±0.3, 0.8±0.3 and 0.8±0.3 ms for each fascicle, respectively as above, and each corresponded to the peak evoked CAP measured on the same electrode. Conduction velocities were 20-60 m/s, which correspond mainly to A and B fibers. The signal-to-noise ratio of evoked averaged peak impedance changes was 16.7±12.4, or 24.5 dB at 6 kHz (n=15 fascicles in N=5 nerves).

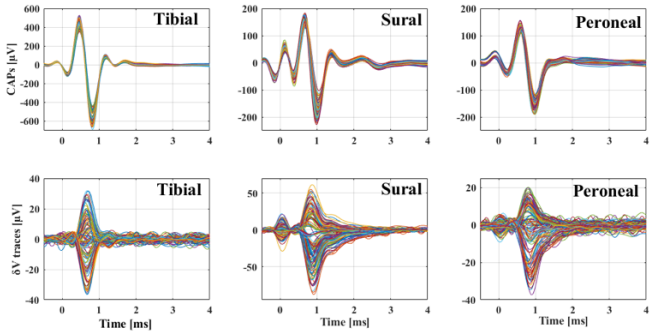

Fig. 2. Representative CAPs and δV traces. CAPs were recorded on all 14 electrodes of the EIT cuff; δV traces were recorded on 14 electrodes × 14 current injections = 196 for tibial, sural and peroneal fascicles.

Validation techniques and co-registration. MicroCT imaging allowed for the visualization and clear distinguishability (d=0.998, as in[12]) of the three main fascicles of the rat sciatic nerves and their subsequent segmentation (Fig. 3). The average diameter difference of all three fascicles and the full nerves between microCT and histology was <2.5%. To image the full rat sciatic nerve, 3-4 overlapping scans of ~8 mm length taking 3.5 h each were needed. Images for the three techniques were co-registered by fitting the microCT and neural tracer images to the circular shape of EIT images. This was achieved by rigid deformation and rotational alignment to the fiducial marker of a surgical suture on the nerve cuff (Fig. 4).

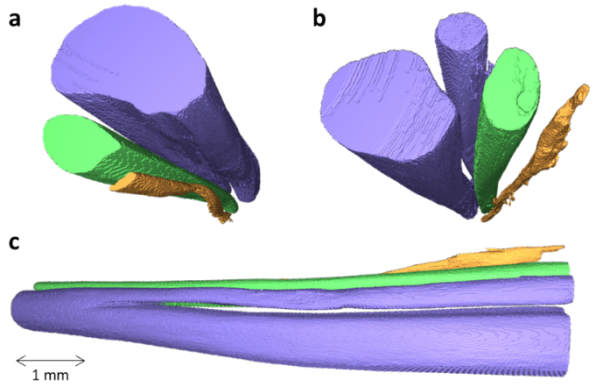

Fig. 3. Example of microCT segmentation of rat sciatic nerve. The segmented tibial (purple large), peroneal (green), sural (purple small, branching off tibial) and post-cutaneous (orange) fascicles can be seen from the **a**, proximal, **b**, distal, and **c**, from proximal to distal (left to right) orientations.

The speed of fluorescent dextran diffusion within the nerve was evaluated and incubation time of 48 h was chosen as optimal (Supplementary Information). Resulting fluorescent images were of high contrast and specificity, with clearly distinguishable boundaries of the fascicles (peroneal and tibial) at the level of EIT cuff placement (Fig. 4b).

Comparison of EIT images with microCT and neural tracing. Three clearly distinct zones of activation due to stimulation of tibial, peroneal and sural fascicles were apparent in reconstructed EIT images for each nerve (Fig. 4a). All recordings had significant peak δV variations related to evoked activity ($p<0.05$). Of 196 available transfer impedances per data set, some were excluded because of low SNR. 146±10 δV traces were then used for EIT image reconstruction. Visual inspection indicates a close correlation of the three fascicles across different techniques. (Fig. 4 and Fig. 5).

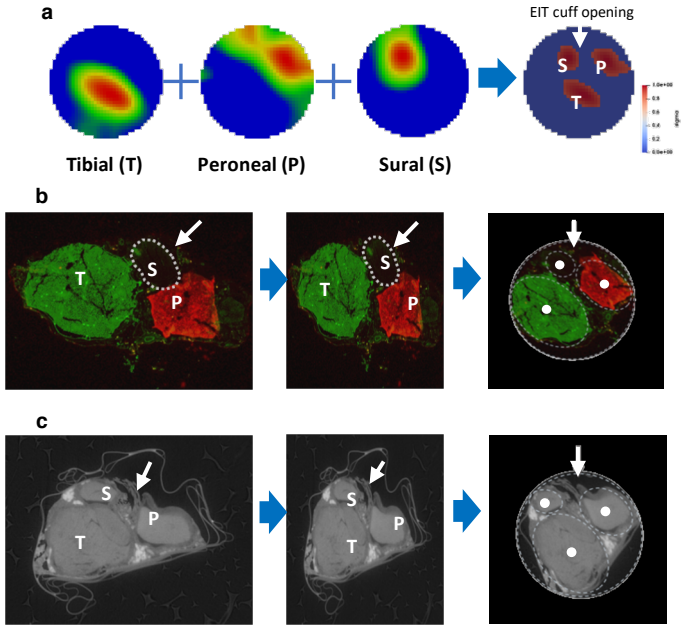

Fig. 4. Examples of co-registration of fascicle angular location with three techniques. **a**, Individual images of evoked fascicular activity reconstructed from EIT recordings and the merged image of reconstructed top 10% activations for all three fascicles. **b**, *Left*: fluorescent image of the cross-section of the common sciatic nerve at the area corresponding to EIT recordings with tibial fascicle labelled with fluorescent Dextran-Alexa 488 (green) and peroneal fascicle with Dextran-Alexa 555 (red). The margins of the sural fascicle which did not receive tracer injection are demarcated with a dashed line. *Middle:* rigid deformation. *Right*: rotation of histology image for purposes of cross-validation of CoM of fascicles between three techniques. The external boundaries of the nerve were fitted to a circular profile after rigid deformation. Each fascicle was fitted into an ellipsoid profile (dashed white line) with a CoM (white dot in the middle) which was further used as a ground truth coordinate in the cross-validation study. **c**, *Left*: representative XY plane slice of the microCT scan of the nerve in the area corresponding to EIT recordings with fascicles clearly visible and snippets of the silk thread marking the EIT cuff opening area (pointed at with white arrow). *Middle and right*: rigid deformation and rotation of microCT image for co-registration.

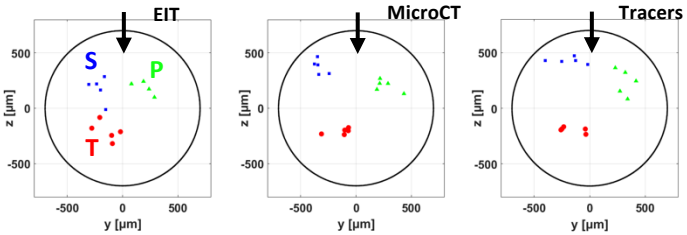

Fig. 5. Centers of mass of fascicles. CoMs derived for all three techniques (N=5 nerves) oriented to position the fiducial marker (cuff opening) at 12 o'clock (black arrow); red/green/blue dots for tibial, peroneal, sural fascicles, respectively. The nerve boundary is shown as a black circle.

Objective assessment was made using analysis of the radial and angular positions of the center of mass (CoM) of each fascicle. There was significant separation between the fascicles ($p<0.01$ for all three fascicles and three techniques, two-way ANOVA), and no significant difference between the techniques ($p>0.05$, two-way ANOVA). Scatter around the mean fascicle position was 86, 66 and 84 μm (6.2, 4.7 and 6.0% of the nerve diameter), for EIT, microCT, and neural tracer histology respectively.

Discussion

Summary of the results. Fast neural EIT successfully produced images of localized compound action potential in peripheral nerve which correspond to fascicular activity. Evoked impedance changes had a signal-to-noise ratio of 17 for the imaged A and B fast myelinated fibers, applying 6 kHz current. The mean error in fascicle location was 5-6% of nerve diameter and similar for each technique. We also developed microCT and neural tracing with fluorescent dextran conjugates to be suitable for independent validation. These allowed successful identification of individual fascicles at the distal sites of their anatomical projections and reliable tracing proximally to the level of common sciatic nerve where the EIT cuff electrode was positioned. Upon histological examination of the cross-sections at the level of EIT cuff, the fluorescent dextran conjugates were shown to label the entire target fascicle and clearly demarcate the boundaries of the nerve (no fluorescence observed in epineurium).

Technical considerations. Fast neural EIT in the cerebral cortex has been validated by comparison to the independent techniques of local field potentials, current source density and intrinsic optical activity[35]. Here, we present the first validation of fast neural EIT in peripheral nerve. EIT is a soft-field imaging modality and so typically has a spatial resolution of ~10% of the image diameter. It thus can provide a unique localized image of neuronal depolarization but it is not necessarily restricted to individual fascicles. The other two methods were chosen in order to demonstrate a correspondence with the fascicular localized activity which might be expected on physiological grounds. The independent methods also have intrinsic geometric errors which necessarily result from the tissue fixation procedure, consequent deformation of the tissue and the need to deform the resulting images for co-registration. The overall mean percentage shrinkage of formalin-fixed tissue compared to the fresh specimen, for example, is ~10% but can vary depending on tissue type and fixation duration. For example, shrinkage of solid tumor tissue specimens varies between 4.6-11.2%[36], whereas the longitudinal shrinkage of an optic nerve after formalin fixation was reported to reach 30%, and this value varied with the age of patients (higher with younger age)[37]. Nevertheless, there appears to be a good correlation between fascicles and techniques of ~10% of nerve diameter which is reasonable for typical experimental error[35].

Comparison to inverse source analysis (ISA). EIT and ISA are mathematically similar but EIT has several advantages: unlike in ISA, the electric source in EIT is known, thus, there is a unique inverse solution; EIT allows collection of more independent data: for n electrodes, there are $O(n^2)$ independent measurements, compared to O(n) measurements for ISA. Another significant advantage of EIT over ISA is that is has no field cancellation problem: impedance changes due to ion channel opening are highly unimodal and so any cancellation of signals with EIT is negligible, whereas in ISA, positive and negative fields may cancel without reaching surface electrodes[22]. Early attempts at fascicle localization with ISA achieved only partial success. Activity in multiple pathways could only be successfully localized in 25% of cases[38] when using 56 electrodes in a matrix configuration around the rat sciatic nerve. More recent advances are mainly associated with the FINE neural cuff electrode[39], which constrains the nerve into a rectangular cross-section. Modelling and tank studies suggested ~1 mm localization accuracy using FINE electrodes with 16 contacts around the dog sciatic nerve[40-42]. Repeatability of fascicle imaging with ISA is also unclear. Wodlinger et al[43] reconstructed source locations overlaid on histology in three of the seven nerves studied. Of the six fascicles represented, one was completely off, and three were largely outside the histological fascicle.

Physiological considerations. In the brain, the highest signal-to-noise ratio has been found empirically to be at 1.7 kHz. At lower frequencies, the impedance evoked voltages are contaminated by endogenous potential activity, such as the EEG, evoked potentials or seizure activity. At higher frequencies, the impedance change reduces as more applied current crosses through the neuronal membrane at rest so there is less difference as ion channels open during activity. In this work, a higher applied frequency of 6 kHz has been found to provide the highest SNR. This may be attributed to the higher component frequencies in the compound action potential and the differing biophysics of myelinated nerve fibers. The effect has been confirmed in a biophysical model of impedance changes during the compound action potential in peripheral nerve[26]. A concern when undertaking impedance measurement is that the applied current might itself cause changes in voltage sensitive ion channels and alter neuronal excitability. The current used in this work was 60 μA at 6 kHz. It was shown that current of up to double this has a negligible effect on neuronal excitability; this was borne out in these studies, as there was no effect on the averaged compound action potential recorded[26].

The changes recorded in this study were only of larger myelinated A and B fibers. For use in autonomic nerve studies, this poses a limitation, as the majority are slow conducting C fibers. Similar impedance changes occur in unmyelinated nerve and have been demonstrated in the walking leg nerve of the crab[44]. The frequency for recording these is different and probably optimal at 225 Hz[45]. A challenge of EIT of these fibers is dispersion - the impedance change may become vanishingly small more than 10 cm from the initiation site. This may pose a limitation to application in long unmyelinated nerve activity. However, recent modelling in our group has indicated that this too may be possible with sophisticated signal processing and longer averaging times[46].

In this work, averaging took 14 minutes for each image data set. This does not pose a problem if it is possible to stimulate peripheral branches continually for several minutes. However, in this work a SNR of ~17 was produced. It may still be possible to produce good EIT images with shorter averaging. Depending on the application, it may well be practicable to collect data and average over longer periods of hours if, as planned, a nerve cuff could be left in situ and record over hours or days. In addition, the SNR could be improved through spatiotemporal methods of activity extraction; for example, velocity-selective[47] or variance-based methods, similar to those used for advanced inverse source analysis algorithms[42].

Future applications. In this study, we have demonstrated the feasibility of using fast neural EIT for imaging fascicular activity within peripheral nerve with a high spatio-temporal resolution and cross-validated the resulting EIT images against neural tracer histology and microCT. This is encouraging to the view that this method might be used to identify fascicles of interest in human Electroceutical activity in the future. This could then enable selective stimulation of identified fascicles using the same nerve cuff. As the vision for the future is that this would occur with implanted devices, the requirement to average over minutes should not be a limitation. The method could be used to monitor and adjust selective stimulation interactively over lengthy periods.

Methods

All experiments were performed in accordance with the European Commission Directive 2010/63/EU (European Convention for the Protection of Vertebrate Animals used for Experimental and Other Scientific Purposes) and the UK Home Office Scientific Procedures Act (1986) with project approval from the University College London Institutional Animal Welfare and Ethical Review Committee.

Neural tracing. Adult male Sprague-Dawley rats (400-450 g) were anesthetized with isoflurane (5% induction, 2% maintenance). The tibial and peroneal branches of the sciatic nerve on both sides were exposed and pressure injected with 3 µL of 2.5% Alexa Fluor 488 or Alexa Fluor 555 dextran 10 kDa (ThermoFisher) in 0.01 M phosphate buffered saline (PBS) using a glass micropipette ~2 cm distal to the branching region of the nerve. The speed of infusion was maintained at 0.5-1 µL/min and the tip of the pipette was left in a position for 2 min after completion of the injection to prevent tracer leakage. The animal recovered for 48 h before EIT recordings to ensure diffusion of the tracer to the level of the common sciatic nerve.

In vivo preparation. Animals were anesthetized with urethane (1.3 g/kg, i.p.), intubated and artificially ventilated using a Harvard Apparatus Inspira Ventilator (Harvard Apparatus, Ltd, UK) with a 50/50% gas mixture of O2 and air. Electrocardiogram and respiratory parameters (respiratory rate, end tidal CO2) were monitored (Cardiocap 5, Datex Ohmeda). The core body temperature of the animal was controlled with a homeothermic heating unit (Harvard Apparatus, Kent, UK) and maintained at 37°C. The animal was positioned prone and access to the common sciatic nerve was gained by dividing the biceps femoris and vastus lateralis muscles. Access to the posterior tibial nerve was established through dividing tibialis anterior and extensor digitorum longus muscles. The common peroneal nerve was accessed through a 2 mm lateral incision in biceps femoris near the knee joint. Sural nerves were dissected from their origin from sciatic nerves to the lateral malleolus. Stimulation cuff electrodes (CorTec Gmbh, Freiburg, Germany) coated with PEDOT:pTS were placed around the three branches, and an EIT cuff (see subsection "*Electrode design*") was placed around the main trunk of the sciatic nerve. After that, the retainers were removed, and surgical incision areas were closed with cotton pads soaked in 0.9% sterile saline solution. When the surgical procedure was completed, the animal was given pancuronium bromide (0.5 mg/kg, i.m.) to avoid movement artefacts.

Fast neural EIT: electrode design. Flexible custom-made EIT cuff electrode arrays were made from laser cut stainless steel foil (12.5 µm thick) on medical-grade silicone rubber[28]. Arrays comprised two rings of 14 0.14x1 mm pads and two reference ring electrodes placed at extremities of the cuff. The 14 electrodes over each ring-like arrangement were equally spaced, thus radial distance between adjacent pads was ≈25.7°. The distance between electrode arrays was 2 mm (gap between centers), and the distance between each electrode array and closest reference electrode was 2.2 mm (edge-to-edge). Only one reference electrode and one 14-electrode ring was used for the recording EIT in these experiments (the second ring and second reference electrode are part of the design to allow compatibility of the cuff with other applications such as selective stimulation and imaging, which are not part of this publication). The cuff is designed to wrap around a nerve 1.4 mm in diameter. Electrodes were coated with poly(3,4-ethylenedioxythiophene):p-toluene sulfonate (PEDOT:pTS) to reduce contact impedance and noise from the electrode-electrolyte interface[28]. To stabilize the cylindrical shape of the array and to secure the cuff around the nerve, the array was glued onto the inner side of a 1.5 mm internal diameter (I.D.) silicone rubber tube to form a 1.4 mm I.D. cuff, with thread sutured to assist cuff opening during implantation. The connector side was attached to a custom-printed circuit board adapter using 30 pin 1.5 mm connectors (Farnell, UK).

Fast neural EIT: electric stimulation of the fascicles and impedance measurements. Recordings of the evoked activity in tibial, peroneal and sural fascicles of the sciatic nerve were performed using the EIT cuff electrode array placed over the common part of the nerve. Branches were individually stimulated supramaximally at 1-2 mA amplitude, 5 Hz frequency, 50 µs pulse width with CorTec cuff tunnel bi-polar electrodes (CorTec GmbH, Germany) placed ~1-1.5 cm distally from the EIT cuff (Fig. 1). A current of 1-2 mA was chosen to maximize the magnitude ratio between the CAP and the stimulus artefact measured on the EIT cuff electrode array prior to EIT recordings. The EIT protocol comprised 14 current injections (4-off spacing drive pattern, or ≈100°, Fig. 1b), each 60 s long, 300 trials averaged over each injection, with 14 min averaging in total. The injected current frequency and amplitude was 6 kHz and 60 µA, respectively. Averaging over repeated stimulation pulses was required to reduce noise and reach a SNR sufficiently high for successful imaging. EIT measurements were performed with a ScouseTom system[31]. Raw signals were converted to δV recordings ("traces", Fig. 1b) by Hilbert transform demodulation (magnitude-only) at ±2 kHz bandwidth around the 6 kHz EIT carrier.

Criteria for exclusion of collected impedance traces from subsequent reconstruction process were as follows:

- Injection/measurement on faulty electrode (characterised by extremely high noise compared to the rest of the electrodes).
- DC saturation of raw signal.
- δV background noise >3 µV.

Fast neural EIT: image reconstruction. EIT images were reconstructed using the following procedure[25,29,48].

The forward problem solution was computed using a complete electrode model (CEM) within the UCL PEITS fast parallel forward solver[49]. The electrode contact impedance value in the solver was set to 1 KΩ, and EIT current 60 μA. An extended forward model was used[29]; compared to the basic cylindrical model employed in our previously published proof-of-concept study[25], it included an additional external subdomain largely more conductive than the nerve itself. The new subdomain was included after observing that the original model simulated boundary voltages did not properly correlate with experimental ones due to the leakage of the electrical current at the edges of the cuff. A cylindrical model of the nerve with uniform baseline conductivity was set to 0.3 S/m, the external environment of the nerve was accounted for with higher conductivity (1.5 S/m), and cuff electrodes were placed over the external surface of the nerve. This geometrical design was converted to a 2.63M-elements tetrahedral mesh for the purpose of computing the forward solution. The mesh element size and quality were as described previously[29]. The forward solution provided a linearized Jacobian matrix J relating voltage traces δV measured at the electrodes to variations in conductivity (δσ): $\delta V = J \cdot \delta\sigma$[29].

Inverse problem. To image local conductivity changes, a Jacobian matrix J obtained from the forward solution was converted into a coarse hexahedral mesh of voxel size 40 μm and inverted using 0^{th}-order Tikhonov regularization with noise-based voxel correction[25,50]. Only measurements on the single ring of electrodes of the EIT cuff (same ring where EIT current was injected) were used (Fig. 1b and Fig. 6a), for a total of 196 measurements (14 current injections x 14 electrodes), minus traces excluded according to the criteria listed in section 2.5.2 above.

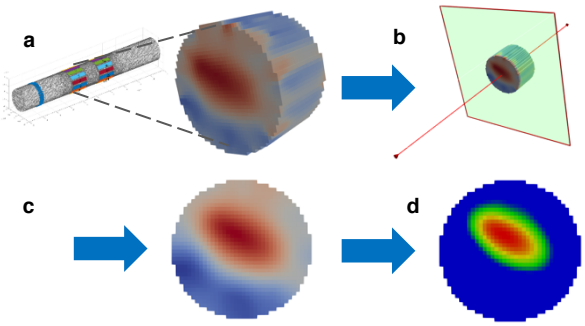

Fig. 6. Post-processing of the reconstructed EIT image. **a**, Nerve subdomain of the 2.63M-elements tetrahedral mesh and zoom-in of conductivity variation reconstructed over the coarse version of the electrode ring used for the EIT protocol. **b**, Selection of the slice on the edge of EIT ring, on the side closest to the reference ring. **c**, Slice-based median and mean filtering. **d**, Normalization, rainbow color map, and FWHM intensity scaling.

EIT reconstructions were evaluated at the time of peak average variations in measured voltage δV (Fig. 1b). Background inter-stimulus noise was also projected into the volume using the same reconstruction parameters. For each reconstruction, each voxel was divided by the standard deviation of projected noise, resulting in the z-score of the conductivity perturbation with respect to the background noise. Reconstruction was performed only on a relevant subset of ≈40K-elements on the hexahedral mesh, namely the part of the nerve subdomain including the injection/measurement ring, as shown in Fig. 6b. Visualization of reconstructed images was performed using Paraview (Kitware, New Mexico, USA).

Images were evaluated at the cross-sectional slice on the edge of the EIT electrode array, as found to be optimal from simulations and previous studies[29]. Reconstructed slices were post-processed with median and mean filtering of 1- and 3-voxels radius, respectively (Fig. 2c). Center-of-mass (CoM) was computed for each fascicle at Full-Width at Half-Maximum (FWHM); for each slice only the top 50% (magnitude) of voxels were included in the computation of metrics (Fig. 2d). This approach was chosen in order to avoid the evaluation being affected by the noise and small artefacts inherent to all reconstructed images.

Tissue collection and processing. At the end of the *in vivo* experiment, the rat was euthanized and the sciatic nerves together with the branches (tibial, peroneal and sural) were excised, fixed in 10% formalin (Sigma Aldrich) and stained with iodine for microCT scanning (see below). To enable co-registration, prior to removal of the EIT cuff, the opening area of the cuff was labelled; after removal of the cuff, a 6.0 surgical silk suture was glued to the epineurium to demarcate the cuff opening. The suture remained in place after all fixation and staining procedures (Fig. 4c). When microCT scanning was complete, the nerves were soaked in PBS to ensure washout of the excess of iodine solution. The nerves were then embedded in paraffin and transversely sectioned at 4 μm. Hematoxylin and eosin (H&E) staining was performed on some sections corresponding to the area of EIT recordings, whereas some sections were cover-slipped with fluorescence-preserving medium for direct histological analysis of fluorescent neural tracers. Fluorescent images were obtained using a Leica microscope at 10x. The sural fascicle was located by visual inspection and identified by the absence of the fluorescent tracer which labelled the peroneal and posterior tibial fascicles.

MicroCT scanning and image analysis. Following fixation, the sciatic nerve was stained in 1% Lugol's iodine solution (total iodine 1%; 0.74% KI, 0.37% I, Sigma Aldrich) for 24 h. After staining, the nerve was blotted dry to remove excess iodine solution and wrapped into a piece of cling film to avoid shrinkage of the nerve tissue during scanning. The nerve was then pulled in a taut position and fixed with a cylindrical sponge matrix within a custom-made 3D-printed plastic mount which was placed into a microCT scanner[12]. The microCT scanner (Nikon XT H 225, Nikon Metrology, Tring, UK) was homed and conditioned at 200 kVp for 10 min before scanning. The scanning parameters were optimized previously for highest image quality and contrast[12]. All nerves were scanned using a molybdenum target, a power of 4 W, 2903 projections and a resolution with isotropic voxel size of 4 μm; the scanning parameters were set to 35 kVp energy, 114 μA current and 4 s exposure time (0.25 frames per second). Scans were reconstructed using Nikon CT Pro 3D software (Nikon Metrology, Tring, UK). Center of rotation was calculated manually and beam hardening correction was performed with a preset of 2 and coefficient of 0.0. The reconstructions were saved as 16-bit volumes and triple TIFF

16-bit image stack files. Reconstructed microCT scan images were analysed in ImageJ in the XY plane to view the cross-section of the nerve. Distinguishability (d) between the greyscale values of the soft tissue types (fascicles, interfascicular epineurium and adipocytes) to confirm successful identification of fascicles was calculated[12]. Computerized 3D tracking and segmentation was performed as in[12].

Image co-registration and statistical analysis. A total of eight rat sciatic nerves, from four animals, were used for the recordings of which five nerves were successful; yielding a full dataset with a combination of all three techniques. The other three nerves were excluded from the co-registration analysis due to failure of the neural tracing procedure in one of the fascicles or absence of the compound action potential of impedance signal. Of the 5 nerves used, 4 were on the right and 1 on the left side. The images from the single left sided nerve were flipped in the horizontal plane to allow for combination of all nerves in the same dataset. Centers of mass (CoMs) from EIT images were compared with CoMs from microCT scans and from histology slices with fluorescent neural tracing (referred to as "histology" here). Fascicular CoMs from reference microCT scans and histology images were evaluated by fitting the nerve external boundary to a circular profile after rigid image deformation and manual co-registration of the nerve cuff's opening (marked with the suture glued to the surface of the nerve) by image rotation (example of co-registration process is given in Fig. 4). CoMs from EIT, histology and microCT were compared over vector distance modulus and over radial coordinates (R/ϑ).

A paired *t*-test was performed on peak δV traces with respect to background inter-stimulus noise to determine the significance of impedance changes. Two-way ANOVA was used to evaluate the angular position of the CoM as a function of two independent factors: type of fascicle (tibial, peroneal and sural) and measurement technique (EIT/tracers/microCT). Scatter of fascicle data clusters was computed for each fascicle type and technique as the standard deviation around mean fascicle position, along both coordinate axes. Resulting values were averaged to obtain mean scattering for each technique. Values are presented as mean ± 1 SD unless otherwise stated.

References

1 Hammer, N. *et al.* Cervical vagus nerve morphometry and vascularity in the context of nerve stimulation - A cadaveric study. *Sci. Rep.* **8**, 7997-7997 (2018).
2 Thompson, N., Mastitskaya, S. & Holder, D. Avoiding off-target effects in electrical stimulation of the cervical vagus nerve: Neuroanatomical tracing techniques to study fascicular anatomy of the vagus nerve. *J. Neurosci. Methods* **325**, 108325 (2019).
3 Rangavajla, G., Mokarram, N., Masoodzadehgan, N., Pai, S. B. & Bellamkonda, R. V. Noninvasive Imaging of Peripheral Nerves. *Cells Tissues Organs* **200**, 69-77 (2014).
4 Sahyouni, R. *et al.* Functional and Histological Effects of Chronic Neural Electrode Implantation. *Laryngoscope Investig Otolaryngol* **2**, 80-93 (2017).
5 Beekman, R. & Visser, L. H. High-resolution sonography of the peripheral nervous system – a review of the literature. *Eur. J. Neurol.* **11**, 305-314 (2004).
6 Soldatos, T. *et al.* High-Resolution 3-T MR Neurography of the Lumbosacral Plexus. *Radiographics* **33**, 967-987 (2013).
7 Scopel, J. F. *et al.* Are human peripheral nerves sensitive to X-ray imaging? *PLoS One* **10**, e0116831 (2015).
8 Caldas-Magalhaes, J. *et al.* Validation of Imaging With Pathology in Laryngeal Cancer: Accuracy of the Registration Methodology. *Int. J. Radiat. Oncol. Biol. Phys.* **82**, e289-e298 (2012).
9 Stauber, M. & Müller, R. in *Osteoporosis: Methods and Protocols* (ed Jennifer J. Westendorf) 273-292 (Humana Press, 2008).
10 Yan, L. *et al.* Iodine and freeze-drying enhanced high-resolution MicroCT imaging for reconstructing 3D intraneural topography of human peripheral nerve fascicles. *J. Neurosci. Methods* **287**, 58-67 (2017).
11 Zhu, S. *et al.* Three-dimensional Reconstruction of the Microstructure of Human Acellular Nerve Allograft. *Sci. Rep.* **6**, 30694 (2016).
12 Thompson, N. *et al.* MicroCT optimisation for imaging fascicular anatomy in peripheral nerves. *J. Neurosci. Methods* **338**, 108652 (2020).
13 Mi, D. *et al.* Injection of Fluoro-Gold into the tibial nerve leads to prolonged but reversible functional deficits in rats. *Sci. Rep.* **9**, 9906 (2019).
14 Fritzsch, B. Fast axonal diffusion of 3000 molecular weight dextran amines. *J. Neurosci. Methods* **50**, 95-103 (1993).
15 Murlidharan, G., Samulski, R. J. & Asokan, A. Biology of adeno-associated viral vectors in the central nervous system. *Front. Mol. Neurosci.* **7**, 76 (2014).
16 Towne, C., Montgomery, K. L., Iyer, S. M., Deisseroth, K. & Delp, S. L. Optogenetic control of targeted peripheral axons in freely moving animals. *PLoS One* **8**, e72691-e72691 (2013).
17 Holder, D. S. *Electrical impedance tomography : methods, history, and applications*. 1st Eidition edn, (Francis & Taylor, 2005).
18 Frerichs, I. *et al.* Regional lung perfusion as determined by electrical impedance tomography in comparison with electron beam CT imaging. *IEEE Trans. Med. Imaging* **21**, 646-652 (2002).
19 Cherepenin, V. A. *et al.* Three-dimensional EIT imaging of breast tissues: system design and clinical testing. *IEEE Trans. Med. Imaging* **21**, 662-667 (2002).
20 Clay, M. T. & Ferree, T. C. Weighted regularization in electrical impedance tomography with applications to acute cerebral stroke. *IEEE Trans. Med. Imaging* **21**, 629-637 (2002).
21 Dowrick, T., Blochet, C. & Holder, D. In vivobioimpedance changes during haemorrhagic and ischaemic stroke in rats: towards 3D stroke imaging using electrical impedance tomography. *Physiol. Meas.* **37**, 765-784 (2016).
22 Witkowska-Wrobel, A., Aristovich, K., Faulkner, M., Avery, J. & Holder, D. Feasibility of imaging epileptic seizure onset with EIT and depth electrodes. *Neuroimage* **173**, 311-321 (2018).
23 Hannan, S., Faulkner, M., Aristovich, K., Avery, J. & Holder, D. Frequency-dependent characterisation of impedance changes during epileptiform activity in a rat model of epilepsy. *Physiol. Meas.* **39**, 085003 (2018).
24 Faulkner, M., Hannan, S., Aristovich, K., Avery, J. & Holder, D. Feasibility of imaging evoked activity throughout the rat brain using electrical impedance tomography. *Neuroimage* **178**, 1-10 (2018).
25 Aristovich, K. *et al.* Imaging fast neural traffic at fascicular level with electrical impedance tomography: proof of principle in rat sciatic nerve. *Journal of Neural Engineering* **15**, 056025 (2018).
26 Tarotin, I., Aristovich, K. & Holder, D. Simulation of impedance changes with a FEM model of a myelinated nerve fibre. *Journal of Neural Engineering* **16**, 056026 (2019).
27 Tarotin, I., Aristovich, K. & Holder, D. Effect of dispersion in nerve on compound action potential and impedance change: a modelling study. *Physiol. Meas.* **40**, 034001 (2019).
28 Chapman, C. A. R. *et al.* Electrode fabrication and interface optimization for imaging of evoked peripheral nervous system activity with electrical impedance tomography (EIT). *Journal of Neural Engineering* **16**, 016001 (2018).
29 Ravagli, E., Mastitskaya, S., Thompson, N., Aristovich, K. & Holder, D. Optimization of the electrode drive pattern for imaging fascicular compound action potentials in peripheral nerve with fast neural electrical impedance tomography (EIT). *Physiol. Meas.* **40**, 115007 (2019).
30 Hope, J., Aristovich, K., Chapman, C., Vanholsbeeck, F. & McDaid, A. in *2019 9th International IEEE/EMBS Conference on Neural Engineering (NER)*. 332-335.

31 Avery, J., Dowrick, T., Faulkner, M., Goren, N. & Holder, D. A Versatile and Reproducible Multi-Frequency Electrical Impedance Tomography System. *Sensors (Basel)* **17**, 280 (2017).
32 Grinsell, D. & Keating, C. P. Peripheral Nerve Reconstruction after Injury: A Review of Clinical and Experimental Therapies. *Biomed Res Int* **2014**, 13 (2014).
33 Raspopovic, S. *et al.* Restoring Natural Sensory Feedback in Real-Time Bidirectional Hand Prostheses. **6**, 222ra219-222ra219 (2014).
34 Hope, J., Vanholsbeeck, F. & McDaid, A. A model of electrical impedance tomography implemented in nerve-cuff for neural-prosthetics control. *Physiol. Meas.* **39**, 044002 (2018).
35 Aristovich, K. Y. *et al.* Imaging fast electrical activity in the brain with electrical impedance tomography. *Neuroimage* **124**, 204-213 (2016).
36 Tran, T. *et al.* Correcting the Shrinkage Effects of Formalin Fixation and Tissue Processing for Renal Tumors: toward Standardization of Pathological Reporting of Tumor Size. *J. Cancer* **6**, 759-766 (2015).
37 Abramson, D. H., Schefler, A. C., Almeida, D. & Folberg, R. Optic Nerve Tissue Shrinkage During Pathologic Processing After Enucleation for Retinoblastoma. *Arch. Ophthalmol.* **121**, 73-75 (2003).
38 Zariffa, J. *et al.* Use of an Experimentally Derived Leadfield in the Peripheral Nerve Pathway Discrimination Problem. *IEEE Trans. Neural Syst. Rehab. Eng.* **19**, 147-156 (2011).
39 Dweiri, Y. M., Stone, M. A., Tyler, D. J., McCallum, G. A. & Durand, D. M. Fabrication of high contact-density, flat-interface nerve electrodes for recording and stimulation applications. *JoVE*, e54388 (2016).
40 Zariffa, J. in *2014 48th Asilomar Conference on Signals, Systems and Computers.* 293-298.
41 Dweiri, Y. M. *et al.* Stable Detection of Movement Intent From Peripheral Nerves: Chronic Study in Dogs. *Proceedings of the IEEE* **105**, 50-65 (2017).
42 Eggers, T. E., Dweiri, Y. M., McCallum, G. A. & Durand, D. M. Model-based Bayesian signal extraction algorithm for peripheral nerves. *Journal of Neural Engineering* **14**, 056009 (2017).
43 Wodlinger, B. & Durand, D. M. Localization and Recovery of Peripheral Neural Sources With Beamforming Algorithms. *IEEE Trans. Neural Syst. Rehab. Eng.* **17**, 461-468 (2009).
44 Chapman, C. A. R. *et al.* Optimisation of bioimpedance measurements of neuronal activity with an ex vivo preparation of Cancer pagurus peripheral nerves. *J. Neurosci. Methods* **327**, 108322 (2019).
45 Tarotin, I., Aristovich, K. & Holder, D. Model of Impedance Changes in Unmyelinated Nerve Fibers. *IEEE Trans. Biomed. Eng.* **66**, 471-484 (2019).
46 Tarotin, I. *et al.* SPARC: Method for Overcoming Temporal Dispersion in Unmyelinated Nerves for Imaging C Fibres with Electrical Impedance Tomography (EIT). *The FASEB Journal* **34**, 1-1 (2020).
47 Metcalfe, B. W., Nielsen, T. N., Donaldson, N. d. N., Hunter, A. J. & Taylor, J. T. First demonstration of velocity selective recording from the pig vagus using a nerve cuff shows respiration afferents. *Biomedical Engineering Letters* **8**, 127-136 (2018).
48 Aristovich, K. Y., Santos, G. S. d., Packham, B. C. & Holder, D. S. A method for reconstructing tomographic images of evoked neural activity with electrical impedance tomography using intracranial planar arrays. *Physiol. Meas.* **35**, 1095-1109 (2014).
49 Jehl, M. *et al.* A Fast Parallel Solver for the Forward Problem in Electrical Impedance Tomography. *IEEE Trans. Biomed. Eng.* **62**, 126-137 (2015).
50 Ventouras, E. *et al.* Tikhonov Regularization Techniques in Simulated Brain Electrical Tomography. *Biotechnology & Biotechnological Equipment* **14**, 95-99 (2000).

Acknowledgements

This work was supported by the UK Medical Research Council (MRC grant No: MR/R01213X/1) and NIH SPARC (1OT2OD026545-01). A.V.G. is a Wellcome Trust Senior Research Fellow.